Magnetic Configurations and Phase Diagrams of Sub-100-nm NiFe Nanorings

Nadjib Benatmane[1,2], Werner Scholz[1], and T. W. Clinton[1]

[1]Seagate Research, Pittsburgh PA 15222-4215 USA
[2]Department of Physics, Georgetown University, Washington, DC 20057 USA

Using the micromagnetics package MAGPAR, we study the ground states of NiFe nanorings with sub-100-nm lateral dimensions, in zero external field. We solve the Landau–Lifschitz–Gilbert equation for three different initial magnetizations (in plane, out of plane, and vortex) to obtain the lowest energy state. Plotting the total energy as a function of thickness, along with its corresponding magnetostatic and exchange energies, we are able to identify various phase transitions and derive phase diagrams as a function of thickness and outer radius, normalized to the exchange length, for rings with different inner to outer radius ratios. We discuss the results in terms of shape anisotropy and its effect on the magnetostatic and exchange energies. We also compare the results of our numerical method to the phase diagram of a nanodot and the phase diagrams of rings obtained by analytical models. Finally, we present a new ground state configuration, the helix, found along the boundary between the vortex and out of plane phases, where the magnetization is vortex like, but with moments canted along the z direction.

***Index Terms*—Micromagnetics, nanoring, phase diagram.**

I. Introduction

SMALL ferromagnetic structures have attracted a lot of interest due to their potential for application in various magnetoelectronic devices [1]–[3]. Among the many shapes being considered, rings have shown a lot of promise for the storage of flux closure states with negligible stray fields, as the highly energetic vortex core is removed. In that respect, a lot of analytical, numerical, and experimental work has focused on the metastable [4] and ground states of such structures [5]–[7], along with their switching dynamics [6], [8], [9], switching fields [10], [11], and hysteretic behavior [10], [12], [13]. In addition, this particular geometry has allowed for the study of various mechanisms to control the final state of the magnetization [14]–[16]. Yet, little has been done in the way of magnetic phase diagrams that would describe the lowest energy state in terms of dimensions and material parameters [5], [17].

In this paper, we use micromagnetic modeling to systematically study the magnetic ground state (lowest energy state) of nanorings as a function of their dimensions. We limit ourselves to the study of NiFe rings with no crystalline anisotropy in the sub-100-nm lateral dimension regime. By comparing the energy of various magnetization distributions, we are able to obtain a phase diagram as a function of outer radius and thickness for different inner to outer radius ratios. We also discuss some of the attributes of a new helical magnetization configuration and compare the results of our numerical method to those of an analytical model and to the data for a disc [17], [18].

II. Method

A. Micromagnetics

The configuration of the ground state of a micromagnetic structure is dictated by the competition between the various terms contributing to the total energy ($E_{\rm tot}$), and their influence on the orientation of the magnetic spins. The four main contributions to $E_{\rm tot}$ are the magnetostatic energy ($E_{\rm ms}$), the exchange energy ($E_{\rm exch}$), the magnetocrystalline anisotropy energy ($E_{\rm ani}$), and the Zeeman energy ($E_{\rm ext}$).

To solve for the ground state, we use the dynamic Landau–Lifschitz–Gilbert (LLG) equation

$$\frac{dM}{dt} = -\gamma' M \times H_{\rm eff} - \frac{\alpha\gamma'}{M_s} M \times (M \times H_{\rm eff}) \qquad (1)$$

to find the magnetization which will produce the lowest total energy, i.e., we perform an energy minimization. In (1), $M = M(r)$ is the magnetization distribution, M_s is the saturation magnetization, $\gamma' = \gamma/(1+\alpha^2)$ with γ the gyromagnetic ratio and α a dimensionless damping constant, and the effective field $H_{\rm eff}$ is given by

$$\mu_0 H_{\rm eff} = \frac{2A}{M_s}\nabla^2 m + \mu_0 H_{\rm ms} + \mu_0 H_{\rm ext} + \frac{1}{M_s}\frac{\partial \omega_{\rm ani}}{\partial m} \qquad (2)$$

where the terms on the right hand side of (2) are the contributions of $E_{\rm exch}, E_{\rm ms}, E_{\rm ext}$, and $E_{\rm ani}$, respectively, while A is the exchange constant, $m = M/M_s, \omega_{\rm ani} = E_{\rm ani}/V$, and $H_{\rm ms} = -\nabla U$, with U the magnetic scalar potential.

B. Simulation Set Up

For the magnetic material of the nanorings, we assume NiFe with the following material parameters: saturation magnetization $\mathrm{J_s} = 1.0$ T, exchange constant $\mathrm{A} = 1.3 \times 10^{-11}$J/m, magnetocrystalline anisotropy constants $\mathrm{K_1} = \mathrm{K_2} = 0$ J/m^3. We choose a damping constant $\alpha = 1.0$ in order to speed up the convergence of our simulations. Note that, since our material has no crystalline anisotropy, and because there is no external field in our system, $E_{\rm ms}$ and $E_{\rm exch}$ are the only contributions to the total energy.

The simulations were run for a ring geometry, using the finite-element (FE) micromagnetics package MAGPAR [19], [22].

Digital Object Identifier 10.1109/TMAG.2007.892867

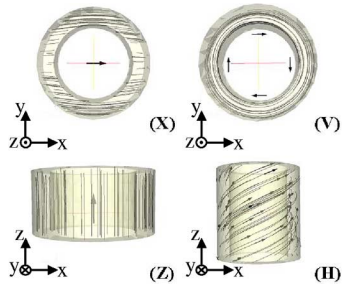

Fig. 1. (a) Magnetic configuration of observed ground states ($\beta = 0.7$). Clockwise from top left: in plane X, vortex V, upward helix H, and out of plane Z. The arrows represent the direction of the total magnetization.

The FE meshes were generated using NETGEN [20], ensuring that for each mesh the average edge length of all the tetrahedral elements was less than the exchange length of NiFe $l_{\text{ex}} = \sqrt{2A/(\mu_0 M_s^2)} = 5.7$ nm. The outer radius R_{out} of the rings ranged between $0.43l_{\text{ex}}$ and $7.9l_{\text{ex}}$, while the thickness t went from $0.08l_{\text{ex}}$ to $15.35l_{\text{ex}}$. For each combination of R_{out} and t, the inner radius R_{in} was selected so that the ratio of inner to outer radius β varied from 0.2 to 0.9.

Starting with a homogeneous magnetization in the x direction (parallel to R_{out}), z direction (parallel to t), or vortex state (clockwise in the xy plane), we let our rings relax in zero external field, solving for and comparing the resulting equilibrium energies. In order to minimize the number of simulations we needed to run, we only looked at points near the phase boundaries, varying the thickness for fixed outer radii. The known phase boundaries for a nanodot [18] were used as a guide. We then plotted the lowest total energy from all three initializations, along with the corresponding magnetostatic and exchange energies, as a function of thickness (Fig. 2). All energies were scaled to the saturation energy density $1/2\mu_0 M_s^2 = 8.042 \times 10^5$ J/m^3.

III. Results

In Fig. 1, we see a representation of all the ground states observed in our simulations. In addition to the in plane (X), out of plane (Z), and vortex (V) states which have been described previously in the literature [5], [6], we also observe a helical (H) state, which will be discussed below. Fig. 2 shows two examples of the plots discussed in the previous section, for a ring with $\beta = 0.6$. One can see the transition from the in plane to out of plane ground state at $t = 1.69l_{\text{ex}}$ (top, $R_{\text{out}} = 1.75l_{\text{ex}}$), illustrated by a discontinuity in the slope of the energy graphs, especially E_{exch}, which drops by an order of magnitude. All β values showed a jump to a lower value of E_{exch} for the transition from the X to the Z phase, except $\beta = 0.2$, which exhibited a jump to a higher value.

This difference in behavior is due to flowering, a configuration where magnetic moments located at the outer edges of the structure open outward (like a flower), to help reduce E_{ms}. $\beta = 0.2$ is the only geometry which needs more flowering out of plane than in plane. The X-Z transitions for the larger β values are for rings with correspondingly smaller surface areas. This reduces the resulting surface charges and, thus, requires less flowering for an out of plane magnetization. For the bottom graph ($R_{\text{out}} = 2.63l_{\text{ex}}$), the transitions are even more obvious, both

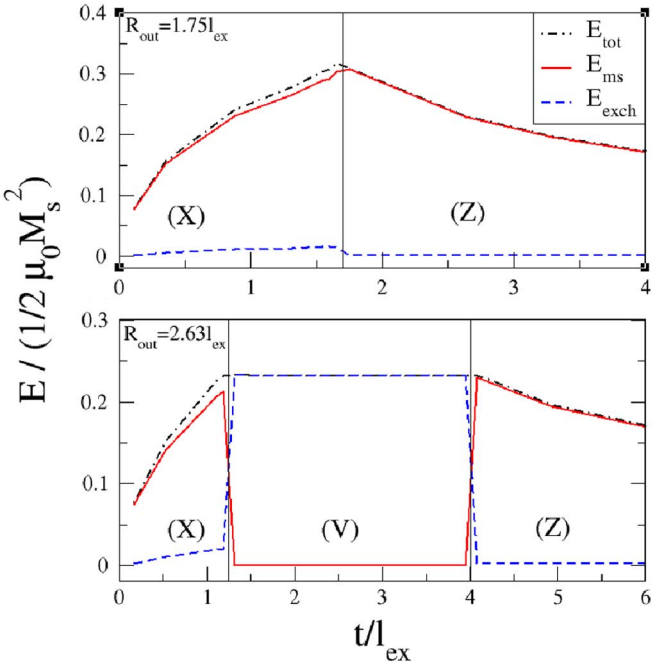

Fig. 2. Plot of E_{tot}, with corresponding E_{ms} and E_{exch} as a function of thickness for $\beta = 0.6$. Top: $R_{\text{out}} = 1.75l_{\text{ex}}$ with a phase transition at $t = 1.69l_{\text{ex}}$. Bottom: $R_{\text{out}} = 2.63l_{\text{ex}}$ with transitions at $t = 1.24l_{\text{ex}}$ and $t = 4l_{\text{ex}}$.

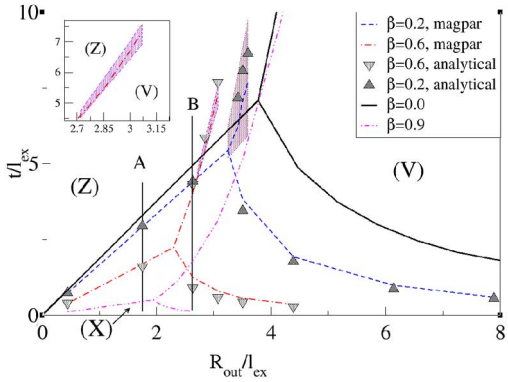

Fig. 3. Comparison of the phase diagram of a nanodot (solid line, $\beta = 0.0$) with the results of MAGPAR (dotted lines, $\beta = 0.2, 0.6, 0.9$) and those of the analytical model [17] (up and down triangles, $\beta = 0.2, 0.6$), along with a representation of the region where the H state is found for these two values of β (shaded areas). Also shown, lines A and B, corresponding to the thickness scans of Fig. 2; inset: magnified view of the H state region for $\beta = 0.6$, which is significantly smaller than the region for $\beta = 0.2$.

as a discontinuity in E_{tot}, and as a cross over between E_{ms} and E_{exch}, occurring at $t = 1.24l_{\text{ex}}$ and $4l_{\text{ex}}$ for the X to V phase and V to Z phase, respectively. These two thickness scans correspond to line A ($R_{\text{out}} = 1.75l_{\text{ex}}$) and line B ($R_{\text{out}} = 2.63l_{\text{ex}}$) in Fig. 3. The above energy transitions are what we observed for all our simulations, and were used to determine the location of the transition points.

The H state has spins aligned along the circumference of the ring in the xy plane (much like the V state), but with nonzero components along the z axis that all point in the same direction (upward in Fig. 1). The spin components normal to the surface near the top and bottom of the ring have smaller magnitudes,

thereby reducing the fringe fields. This state, found in the region around the phase boundary between the V and Z phases, is a dimension dependent intermediate magnetization distribution, similar to the twisted flower state described by Hertel *et al.* [21]. Our results indicate the H ground state is a different phase from the V and Z phases, at least for rings with $\beta > 0.2$. We base this on the fact that for β values greater than 0.2, the H state is only accessible from an initial magnetization in the x direction. This is nowhere near any local minimum of the energy landscape for the region of interest, where we only expect to find minima for the Z and V states. Rings initialized with either a vortex or z direction magnetization stayed in their initial states, even when the H state was energetically more favorable and extremely close. This indicates that the minima for the H, and either the V or Z states, can be close to one another, yet are separated by an energy barrier. Rings with $\beta = 0.2$, along with nanodots ($\beta = 0$), did not for their part display the same behavior. For these β values, the H state was readily accessible from the vortex or z direction initialization in most cases.

In addition, for $\beta = 0.2$ or smaller, the H state is present all along the boundary between the V and Z phases. For all other β values, we do not observe such a state, or at the very least it is not accessible from an in plane magnetization below a given R_{out} value. In the phase diagram of Fig. 3, the H state (shaded region) is not present along the V-Z boundary below $R_{\text{out}} = 2.63 l_{\text{ex}}$ for $\beta = 0.6$.

Another feature of the helix is the fact that the range over which this state exists as a function of thickness increases with increasing outer radius, and is different for different β values.

Finally, in Fig. 3, we present a complete phase diagram as a function of outer radius and thickness, for various β values. We compare them to the phase diagram of a nanodot [18] (solid line). As we can see, removing a bigger portion of the inner core (bigger β values) makes the V state more favorable, compared to an X state, as the energetic vortex core is absent and the exchange energy cost of getting rid of fringe fields is low. One exception is $\beta = 0.9$ where shape anisotropy makes a Z state more favorable over a larger portion of what was once the X state, as the top and bottom surfaces for such a ring are smaller and therefore produce less fringe fields.

We also show a comparison between the results of our numerical method and the analytical model of Beleggia *et al.* [17] for $\beta = 0.2$ and 0.6 (Fig. 3). The phase diagrams obtained from our numerical method (dotted lines) account for nonhomogeneous magnetic states (i.e., flowering), as opposed to the analytical model (up and down triangles), which assumed homogeneous magnetization distributions only. Consequently, the X to V phase transition points are higher in our case, as flowering keeps E_{ms} low enough for the magnetization to stay in the X state, as opposed to the V state which would be more favorable for a homogeneous magnetization. The same reasoning explains why the MAGPAR transition points from the V to Z phase are lower than what the analytical model predicts.

IV. Conclusion

Using a numerical micromagnetic model, we have studied the energy ground states of NiFe rings by running simulations on structures with different initial magnetizations. From our results, we were able to derive phase diagrams as a function of the dimensions of the rings $(R_{\text{out}}, t, \beta)$ with three distinct phases, X, Z, and V. These were discussed in terms of the contributions to E_{tot} and shape anisotropy, and were found to be in good agreement with diagrams obtained from an analytical model. In addition, because we did not impose any restrictions on the final magnetization configurations, we have observed a new helical intermediate state H. It exists at the boundary between the Z and V phases, and presents characteristics of both states, namely a vortex- like orientation of the moments with a cant in the z direction.

References

[1] R. P. Cowburn and M. E. Welland, *Science*, vol. 287, p. 1466, 2000.
[2] J.-G. Zhu and Y. Zheng, *J. Appl. Phys.*, vol. 87, p. 6668, 2000.
[3] M. H. Kryder, W. Messner, and L. R. Carley, *J. Appl. Phys*, vol. 79, p. 4485, 1996.
[4] F. J. Castaño, C. A. Ross, C. Frandsen, A. Eilez, D. Gil, H. I. Smith, M. Redjdal, and F. B. Humphrey, *Phys. Rev. B*, vol. 67, p. 184425, 2003.
[5] C. F. Vaz, C. Athanasiou, and J. A. C. Bland, *Phys. Rev. B*, vol. 73, p. 054411, 2006.
[6] M. Kläui, C. A. F. Vaz, T. L. Monchesky, J. Unguris, E. Bauer, S. Cherifi, S. Heun, A. Locatelli, L. J. Heyderman, Z. Cui, and J. A. C. Bland, *J. Magn. Magn. Mater.*, vol. 272, p. 1631, 2004.
[7] F. J. Castaño, C. A. Ross, A. Eilez, W. Jung, and C. Frandsen, *Phys. Rev. B*, vol. 69, p. 144421, 2004.
[8] M. Kläui, L. Lopez-Diaz, J. Rothman, C. A. F. Vaz, J. A. C. Bland, and Z. Cui, *J. Magn. Magn. Mater.*, vol. 240, p. 7, 2002.
[9] A.-V. Jausovec, G. Xiong, and R. P. Cowburn, *Appl. Phys. Lett.*, p. 052501, 2006.
[10] M.-F. Lai, Z.-H. Wei, J. C. Wu, C. C. Chang, C.-R. Chang, and J.-Y. Lai, *J. Appl. Phys.*, vol. 97, p. 10J711, 2005.
[11] Y. G. Yoo, M. Kläui, C. A. F. Vaz, L. J. Heyderman, and J. A. C. Bland, *Appl. Phys. Lett.*, vol. 82, p. 2470, 2003.
[12] T. A. Moore, T. J. Hayward, D. H. Y. Tse, J. A. C. Bland, F. J. Castaño, and C. A. Ross, *J. Appl. Phys.*, vol. 97, p. 063910, 2005.
[13] F. Giesen, J. Podbielski, T. Korn, M. Steiner, A. van Staa, and D. Grundler, *Appl. Phys. Lett.*, vol. 86, p. 112510, 2005.
[14] M. Kläui, J. Rothman, L. Lopez-Diaz, C. A. F. Vaz, J. A. C. Bland, and Z. Cui, *Appl. Phys. Lett.*, vol. 78, p. 3268, 2001.
[15] L. Lopez-Diaz, M. Kläui, J. Rothman, and J. A. C. Bland, *Phys. B*, vol. 306, p. 211, 2001.
[16] Z. Lu, Y. Zhou, Y. Du, R. Moate, D. Wilton, G. Pan, Y. Chen, and Z. Cui, *Appl. Phys. Lett.*, vol. 88, p. 142507, 2006.
[17] M. Beleggia, J. W. Lau, M. A. Schofield, Y. Zhu, S. Tandon, and M. De Graef, *J. Magn. Magn. Mater.*, vol. 301, p. 131, 2006.
[18] W. Scholz, K. Y. Guslienko, V. Novosad, D. Suess, T. Schrefl, R. W. Chantrell, and J. Fidler, *J. Magn. Magn. Mater.*, vol. 266, p. 155, 2003.
[19] [Online]. Available: http://magnet.atp.tuwien.ac.at/scholz/magpar/
[20] [Online]. Available: http://www.hpfem.jku.at/netgen/
[21] R. Hertel and H. Kronmüller, *J. Magn. Magn. Mater.*, vol. 238, p. 185, 2002.
[22] W. Scholz, J. Fidler, T. Schrefl, D. Suess, R. Dittrich, H. Forster, and V. Tsiantos, *Comput. Mater. Sci.*, vol. 28, pp. 366–383, 2003.

Manuscript received October 31, 2006 (e-mail: mnb24@georgetown.edu).